UCRL-16904

University of California
Ernest O. Lawrence Radiation Laboratory

MEASUREMENTS OF THE YIELD STRESS OF ALLOYS WITH COHERENT LAMELLAR MICROSTRUCTURES (II)

TWO-WEEK LOAN COPY

This is a Library Circulating Copy which may be borrowed for two weeks. For a personal retention copy, call Tech. Info. Division, Ext. 5545

DISCLAIMER

This document was prepared as an account of work sponsored by the United States Government. While this document is believed to contain correct information, neither the United States Government nor any agency thereof, nor the Regents of the University of California, nor any of their employees, makes any warranty, express or implied, or assumes any legal responsibility for the accuracy, completeness, or usefulness of any information, apparatus, product, or process disclosed, or represents that its use would not infringe privately owned rights. Reference herein to any specific commercial product, process, or service by its trade name, trademark, manufacturer, or otherwise, does not necessarily constitute or imply its endorsement, recommendation, or favoring by the United States Government or any agency thereof, or the Regents of the University of California. The views and opinions of authors expressed herein do not necessarily state or reflect those of the United States Government or any agency thereof or the Regents of the University of California.

Submitted to Acta Metallurgica

UCRL-16904

UNIVERSITY OF CALIFORNIA

Lawrence Radiation Laboratory
Berkeley, California

AEC Contract No. W-7405-eng-48

MEASUREMENTS OF THE YIELD STRESS OF ALLOYS WITH COHERENT LAMELLAR MICROSTRUCTURES (II)

S. D. Dahlgren

June 1966

MEASUREMENTS OF THE YIELD STRESS OF ALLOYS WITH COHERENT LAMELLAR MICROSTRUCTURES (II)

S. D. Dahlgren

Inorganic Materials Research Division of
Lawrence Radiation Laboratory,
University of California,
Berkeley, California

ABSTRACT

The yield stresses of polycrystalline Cu-Ni-Fe alloys were measured and compared with values calculated from a theory for the yield stress of alloys with lamellar microstructures. Agreement between theory and experiment was found for the following points: (1) The yield stress is directly proportional to the difference in the cubic lattice parameters of the two structures forming the lamellar microstructures, (2) The yield stress is independent of the volume fractions of the structures present in the Cu-Ni-Fe alloys studied, (3) The yield stress is independent of the interlamellar spacing present. In addition, calculations indicate that the demixing process of spinodal decomposition in Cu-Ni-Fe alloys is inhibited by the coherency strains created during decomposition.

INTRODUCTION

A theory for the yield stress of alloys with coherent lamellar microstructures is presented in Part I of this work.[1] The theory is based on structures which form during spinodal decomposition of Cu-Ni-Fe alloys and therefore alloys from this system were selected for checking the theory. Low temperature decomposition of Cu-Ni-Fe alloys produces two tetragonal structures, one with $c/a < 1$ and the other with $c/a > 1$.[2-4] The "a" parameter is considered to be constant and the same for both structures and the "c" parameter is a function of position through the lamellae for the microstructure of interest. It is assumed in the theory that the tetragonality of the two structures is caused by elastic strains needed to maintain coherency of two structures that, if unattached, would be cubic. Dislocation motion is consequently inhibited by the stresses associated with these elastic strains.

Equations giving the critical resolved shear stress, τ_{app}, are derived in Part I.[1] The critical resolved shear stress can be obtained experimentally from oriented single crystal tensile specimens with the aid of the Schmid factor. However, polycrystalline samples are adequate to check a number of the points of the theory. Absolute values of the tensile yield stress can be calculated on the basis of theories[5] for the plastic deformation of polycrystalline samples which gives

$$\bar{\sigma}_{yield} = \bar{m}\,\tau_{app} \qquad (1)$$

where the constant $\bar{m}$ involves an average orientation factor for the slip systems which operate during plastic flow. For randomly oriented grains, $\bar{m} = 3.06$. When the grains are preferentially oriented, $\bar{m}$ will in general differ from 3.06 but will always be greater than two.

EXPERIMENTAL PROCEDURE

Four compositions of polycrystalline Cu-Ni-Fe samples were prepared and these are designated as alloys 1, 2, 3, and 4 in Fig. 1 and Table I. Compositions were verified by chemical analysis. Alloys 1, 2, and 3 lie on one tie line. The alloys were case into one-half inch diameter copper molds in an inert atmosphere, forged (alloys 1-3) or swaged (alloy 4) to three-eighth inch diameter rod, and homogenized for three days at 950°C in evacuated quartz capsules. Before melting, 0.5 wt.% manganese was added to each alloy to aid fabrication. The average grain size of the homogenized bars was 0.15 mm. Tensile bars with a gauge length of 1.125 inches and diameter of 0.160 inches were ground from the homogenized bars, encapsulated in evacuated quartz tubes, heated to 950°C, and quenched in water before aging.

Alloys 1-3 were aged at 625°C for various times, or aged first at 625°C for a specified time and then given a subsequent treatment at 450°C for 100 hours. Daniel[7] has shown that the length of time at the higher temperature fixes the wavelength of the composition fluctuation while the lower temperature influences the amplitude of the fluctuation. Samples of alloy 4 were aged to their maximum hardness at 800°C, 730°C, and 625°C to independently check the effect of variation in lattice constants of the two precipitating structures. An additional sample of alloy 4 was first aged 6 hours at 625°C and then held 100 hours at 550°C. Errors in determining the maximum yield stress as a function of aging time were not found to be critical because the maximum is very broad for Cu-Ni-Fe alloys (e.g., see Fig. 2). It was necessary to quench the samples after aging at temperatures above 625°C to prevent structural changes from occurring while cooling to room temperature. An Instron

Table I. Compositions of alloys 1-4 with volume fractions, f_1 and f_2, estimated from the phase diagram. Copper-poor structure is indicated by subscript 1.

Alloy	Cu	Ni	Fe	f_1	f_2
1	54.4	36.7	8.9	.25	.75
2	41.8	44.8	13.4	.50	.50
3	30.7	52.5	16.8	.68	.32
4	50	35	15	.43	.57

tensile testing machine was employed to determine the room temperature tensile yield stress. The strain rate was .0175 in/in/min and the yield stresses were determined by the .02% offset method.

Lattice parameters of the two equilibrium phases were determined from alloy 4 for the three aging temperatures, 800°C, 730°C, and 625°C. Powder samples of alloy 4 were held 15 days at 800°C, and one month at 730°C and 625°C. A back reflection focusing camera of 50 mm radius, and unfiltered chromium radiation were used for the lattice parameter determinations.

EXPERIMENTAL RESULTS

Figure 2 shows the measured yield stress versus aging time data for alloy 2. The yield stress reaches its maximum rapidly and maintains a value very near the maximum even after 194 hours at 625°C. The other alloys (1-3) revealed similar trends at 625°C as did the alloys given the additional 450°C treatment, but the yield stresses of tensile specimens given the additional treatment were shifted to higher values. Table II gives the maximum measured values taken from the yield stress vs. aging time curves for alloys 1, 2, and 3 aged at the two temperatures. The aging time to maximum yield was either 8 hours at 625°C, or 8 hours at 625°C plus 100 hours at 450°C. Table III gives the experimental yield stresses for samples of alloy 4 after aging each to its maximum hardness which occurred after holding for 3 minutes at 800°C, 16 minutes at 730°C, and 8 hours at 625°C. The yield stress of the alloy 4 sample which was held at 625°C for 6 hours and then 100 hours at 550°C is also given in Table III.

Table II. Measured and calculated yield stresses for alloys 1-3. Calculated values in the columns with $\overline{m} = 3.06$ and $\overline{m} = 2.75$ are respectively for samples with randomly oriented grains and for samples that have a preferred orientation of grains caused by fabrication.

Alloy	Aging Temp.	Measured Yield Stress	Calculated Yield Stresses $\overline{m} = 3.06$	$\overline{m} = 2.75$
1	625°C	47,150 psi	54,550 psi	49,100 psi
2	625°C	47,150	52,270	47,040
3	625°C	48,030	50,740	45,670
1	450°C	63,820	71,280	64,640
2	450°C	63,050	68,760	61,880
3	450°C	62,900	66,700	60,030

Table III. Measured and calculated yield stresses for alloy 4. Calculated values in the columns with $\overline{m} = 3.06$ and $\overline{m} = 2.5$ are respectively for samples with randomly oriented grains and for samples that have a preferred orientation of grains caused by fabrication.

Alloy	Aging Temp	Measured Yield Stress	Calculated Yield Stresses $\overline{m} = 3.06$	$\overline{m} = 2.5$
4	800°C	29,500 psi	39,770 psi	32,490 psi
4	730°C	40,900	50,330	41,120
4	625°C	53,620	64,880	52,940
4	550°C	62,290	76,220	62,270

DISCUSSION OF RESULTS

Confirmation of Predicted Trends

It is shown in Part I[1] that the critical resolved shear stress is given by

$$\tau_{app} = \frac{1}{\sqrt{6}} \quad \frac{f_1}{(S_{11} + S_{12})} \left(\frac{\Delta a_o}{a_{10}}\right) \tag{2}$$

where the volume fraction f_1 is below the critical value of $\frac{1}{3}$. S_{11} and S_{12} are elastic compliances, a_{10} is the cubic lattice parameter for structure 1, and Δa_o is the difference in the cubic lattice parameters of structures 1 and 2. For volume fractions f_1 between critical values ($\frac{1}{3}$ to $\frac{2}{3}$), the shear stress is given by

$$\tau_{app} = \frac{1}{3\sqrt{6}} \quad \frac{1}{(S_{11} + S_{12})} \left(\frac{\Delta a_o}{\bar{a}}\right) \tag{3}$$

where $\bar{a}$ is calculated from Eq. (4). Equations (2) and (3) were derived under the condition that $(S_{11} + S_{12})_1 = (S_{11} + S_{12})_2$ where the subscripts outside the parentheses refer to the compliances for structures 1 and 2, respectively. When $(S_{11} + S_{12})_1 \neq (S_{11} + S_{12})_2$ and the volume fractions are between the critical limits, the results of Eqs. (4) and (5) can be

$$\bar{a} = \frac{a_{10}a_{20}\left\{f_1(S_{11} + S_{12})_2 + f_2(S_{11} + S_{12})_1\right\}}{a_{20}f_1(S_{11} + S_{12})_2 + a_{10}f_2(S_{11} + S_{12})_1} \tag{4}$$

$$\sigma_{xx} = \frac{\bar{a} - a_o}{(S_{11} + S_{12})\, a_o} \tag{5}$$

$$\tau_{app} = \frac{1}{3\sqrt{6}} (\sigma_{xx1} - \sigma_{xx2}) \tag{6}$$

combined with Eq. (6) to give τ_{app}. The "a" tetragonal lattice parameter that is common to both structures 1 and 2 is designated by $\bar{a}$, a_{20} is the

cubic lattice parameter for structure 2, and σ_{xx} is the maximum tensile stress along the length of individual lamellae.

Experimental verification of the theory is limited to the conditions under which Eqs. (3-6) are applicable, i.e., when the volume fractions are between the critical limits. Three significant points are indicated by Eqs. (3-6) and these will be discussed next.

1. Equation (3) suggests that a plot of measured yield stress versus Δa_o would produce a straight line passing through the origin, i.e., the yield stress is directly proportional to Δa_o. Equation (3) requires that $(S_{11} + S_{12})_1 = (S_{11} + S_{12})_2$ but the proportionality between yield stress and Δa_o is quite constant for any one alloy even if the sums of the compliances are different. This is difficult to establish analytically; however, a graphical example shows it to be true. The points in Fig. 3 designated by squares represent calculated yield stresses ($\bar{m} = 2.5$) which were computed for alloy 4 using Eqs. (4-6) where $(S_{11} + S_{12})_1 \neq (S_{11} + S_{12})_2$. These points lie on the solid line which extrapolates to the origin as required by direct proportionality. Figure 3 shows plots of the measured peak yield stress versus the difference in lattice parameters of the equilibrium cubic phases for alloys 1-3 (circles) and versus the difference in cubic lattice parameters calculated from tetragonal lattice parameter data for alloy 4 (triangles). (The method of evaluating Δa_o from tetragonal data will be discussed later.) The points on both lines are easily within the accuracy of the yield stress data or especially, in the case of alloy 4, within the accuracy of the method of determining Δa_o from tetragonal lattice parameters. The data thus give a confirmation of the direct proportionality between yield stress and Δa_o.

2) The volume fractions of the two precipitating structures are

different for each of the alloys 1-3 although their compositions are the same for any given temperature because these alloys all lie on the same tie line. Table II shows that the maximum yield stress is constant for these three alloys when they have been aged at the same temperature. Therefore the yield stress does not change as a function of the volume fraction. The small changes in the calculated yield stresses (using Eqs. (4-6)) with changes in volume fraction mainly reflect the differences in the elastic compliances of the two structures. Because the experimental yield stresses do not change with changes in volume fraction, the converse is indicated, i.e., there is no difference in the elastic moduli of the two structures. Thus Eq. (3), which shows no dependence upon volume fraction, can be applied.

The conditions under which Eq. (6) is valid were checked for alloys 1 and 3 because they have volume fractions very near the critical values where Eq. (2) becomes applicable. It was found that Eq. (6) could be applied to both alloys within the uncertainty of establishing the volume fractions for alloys which lie on the tie line for alloys 1-3. The experimental results in Table II show Eq. (6) to be valid.

3. The modulation wavelength, λ, does not appear in the equations for calculating τ_{app} although it is considered in the derivation of these equations. This means the yield stress is independent of interlamellar spacing or particle size. The wavelength of the modulated structure is directly related to the aging time.[4,8,9] Values of the modulation wavelength measured by Hillert et al.[9] on their alloy H, an alloy with a composition near to that of alloy 2, are placed in parentheses at the appropriate times in Fig. 2. These wavelengths are given in numbers of atomic planes. It is clear from Fig. 2 that the yield stress does not vary greatly with aging time or modulation wavelength.

Sources of Data

The slopes of the lines in Fig. 3 depend on the proportionality factors of Eqs. (1) and (3) or, in a more complicated way, on Eqs. (1) and (4-6). In order to make calculations using these equations, the required data for Cu-Ni-Fe alloys must be assembled. The sources of these data will be discussed next.

1. Volume fractions were obtained in all cases from the phase diagram with the aid of the lever law. These values are incorporated in Table I with the alloy compositions.

2. The elastic compliances for the component structures were estimated by first assuming that the elastic anisotropy of the copper-rich structure is the same as for pure copper, and that of the copper-poor structure is the same as for pure nickel. Values of Young's modulus were obtained for pure copper and for copper-nickel alloys of about the same composition as that of the precipitating copper-rich structure. The elastic compliances for the copper-rich structure were then estimated by scaling down the pure copper elastic compliance data in the ratio of the Young's modulus of pure copper to the modulus of the copper-nickel alloy. A similar method was used for the copper-poor structure but this time nickel data were scaled up in the ratio of the Young's modulus for pure nickel to that of the proper nickel-iron alloy. This is justified by the equation used for calculating Young's modulus from single crystal elastic data if the anisotropy of the alloy and the pure element are the same, i.e.,

$$\frac{\overline{1}}{E} = S_{11} + \frac{2}{5}\left(S_{12} + \frac{S_{44}}{2} - S_{11}\right) .$$

Table IV. Elastic modulus and compliance data and estimates used to compute yield stresses of aged Cu-Ni-Fe alloys. References are given by lower case letters. Data on lines 3 and 4 were used for yield strength calculations of alloys 1-3, lines 5 and 6 were used with alloy 4.

Line	Material	Young's Modulus 10^6 psi	Elastic Compliances 10^{-12} cm^2/dyne S_{11}	S_{12}	S_{44}	$S_{11} + S_{12}$
1	Nickel	30[a]	.80	-.31	0.84[d]	.49
2	Copper	17[b]	1.49	-.63	1.3[d]	.86
3	65Ni-35Fe	26[a]	.923	-.358		.565
4	70Cu-30Ni	22[c]	1.150	-.485		.665
5	60Ni-40Fe	25[a]	.960	-.370		.590
6	80Cu-20Ni	21 est.	1.205	-.510		.695

a) Taylor, L., Ed., Metals Handbook (American Society for Metals, Cleveland, Ohio, 1948) p. 600.

b) Ibid., p. 906.

c) Ibid., p. 925

d) Mason, Warren P., Physical Acoustics and the Properties of Solids (D. Van Nostrand Co., Inc., Princeton, N. J., 1958) p. 358.

Here $\bar{E}$ is Young's modulus (for polycrystals); S_{11}, S_{12}, and S_{44} are elastic compliances of individual grains; and the 2/5 factor arises from an average grain orientation consideration. The equation shows that a proportional change in each of the elastic compliances will result in an inverse change in $\bar{E}$. The required data for making estimates of the elastic compliances are included in Table IV. The values from lines 3 and 4 of Table IV were used for alloys 1-3, and those from lines 5 and 6 were used for alloy 4 calculations. The sum $S_{11} + S_{12}$ is also included because it regularly appears in the equations.

3. Lattice constants (in kx units) for the cubic phases in equilibrium in alloys 1-3 were obtained from the lattice parameter contours published by Bradley et al.[10] The compositions of the phases in equilibrium at the given temperatures were obtained from the Cu-Ni-Fe phase diagram.[6] The constants obtained from the literature for alloys 1-3 and the cubic lattice parameters which were determined from samples of alloy 4 after they had been annealed at the given temperatures are shown in Table V. Values of $\bar{a}$ calculated from Eq. (4) are also given in Table V.

The lattice parameters measured on the sample of alloy 4 which had been annealed at 800°C agreed with the values obtained by Hargreaves[3] on the same alloy ($Cu_{10}Ni_7Fe_3$) for the same annealing temperature. These parameters are good to approximately four significant figures. In addition, Hargreaves[3] gave tetragonal lattice parameters for $Cu_{10}Ni_7Fe_3$ aged to the tetragonal stage at three temperatures and these parameters are reproduced in Table VI. A comparison of the calculated values of $\bar{a}$ in Table V with the measured values in Table VI shows a fine agreement. This is consistent with the initial assumption that coherency strains are causing the tetragonal distortions.

Table V. Cubic lattice parameters established through data from references 1 and 2 for alloys 1-3 and measured for alloy 4 of the equilibrium cubic phases which form on annealing at the given temperatures. Equation (4) was used to calculate $\bar{a}$.

Alloy	Aging Temp.	Cu-Poor Structure a_{10}	Cu-Rich Structure a_{20}	Δa_o	Calculated $\bar{a}$
1	625°C	3.558 kx	3.577 kx	.019 kx	3.572 kx
2	625°C	3.558	3.577		3.567
3	625°C	3.558	3.577		3.563
1	450°C	3.555	3.580	.025	3.573
2	450°C	3.555	3.580		3.566
3	450°C	3.555	3.580		3.562
4	800°C	3.579Å	3.594Å	.015Å	3.587Å
4	730°C	3.574	3.597	.023	3.586
4	625°C	3.570	3.600	.030	3.585

Table VI. Tetragonal lattice parameter data from Hargreaves[3] used to calculate the cubic lattice constants of the structures which form in alloy 4 samples during the second stage of decomposition. Values indicated by asterisks were obtained from the graph in Fig. 4. Equation (7) was used to calculate a_{10} and a_{20}.

Aging Temp.	$\bar{a}$	Cu-Poor Structure $c_1/\bar{a}$	Cu-Rich Structure $c_2/\bar{a}$	Calculated Values a_{10}	a_{20}	Δa_o
800°C	3.586A	.995	1.005	3.578Å	3.593Å	.015Å
730°C*	3.586			3.576	3.595	.019
650°C	3.586	.993	1.008	3.575	3.598	.023
625°C*	3.586			3.573_7	3.598_3	.025
500°C	3.586	.991	1.010	3.572	3.601	.029

Hargreaves' tetragonal lattice parameters, $\bar{a}$ and c, were substituted into Eq. (7)[1] to establish the cubic lattice parameters given in Table VII for the constituents making up the lamellar microstructure.

$$a_o = \frac{1}{S_{11}-S_{12}} \left\{ (S_{11} + S_{12})c - 2s_{12}\bar{a} \right\} \qquad (7)$$

The difference in measured and calculated cubic parameters shows an effect which has been mentioned previously.[1] Because the values are given for different temperatures in Tables V and VI, the comparison can best be made on a graph. Figure 4 shows that the cubic parameters calculated from tetragonal lattice parameter data (dashed line) lie inside the measured cubic lattice parameter data (solid line) except at the highest temperature. This indicates that strain energy which increases at low temperatures during the tetragonal stage of the transformation inhibits the approach of the two structures to their equilibrium compositions. Strain energy increases with the square of the strain and therefore becomes significant at larger strains. The method of calculating a_o's from tetragonal data (Eq. (7)) appears to be right because of the close agreement of the calculated values with the measured values at the smaller strain, i.e., for the alloy aged at 800°C. The values of a_o used to determine Δa_o at 625°C and 730°C for the graph in Fig. 3 were taken at the appropriate temperatures from the dashed lines in Fig. 4.

Calculated Yield Stresses

Calculated yield stresses which appear in Table II for alloys 1-3 were obtained using Eqs. (1) and (4-6). In this case $\bar{a}$ was obtained from the cubic lattice parameters using Eq. (4). The calculated yield stresses for alloy 4, Table III, were obtained using the measured tetragonal $\bar{a}$ parameters while a_o's were computed from Eq. (7). Direct

substitution of a_{10}, a_{20}, and $\bar{a}$ in Eq. (5), and use of Eqs. (1) and (6) gave the desired results for alloy 4. Two values of $\bar{m}$ (Eq. 1) were used. The calculated yield stresses given in the column of Tables II and III with $\bar{m} = 3.06$ are for polycrystalline bars with randomly oriented grains. The values in Table II with $\bar{m} = 2.75$ and Table III with $\bar{m} = 2.5$ take into consideration the preferred orientation which occurred during fabrication. These two particular values of $\bar{m}$ were selected because they gave the best fit to the data.

The samples used in checking the theory were forged or swaged which gives rise to a texture with some grains having [100] near the tensile axis and others with [111] parallel to the bar axis.[11] This texture is retained after annealing.[12] The Schmid factor for [100] crystals would be equivalent to using $\bar{m} = 2.45$ while that for [111] grains would correspond to $\bar{m} = 3.68$. Because [100] is the more favorable orientation of the two for slip, grains in this orientation will contribute more to the initial yielding process. Therefore an $\bar{m}$ constant between 2.45 and 3.06 would be appropriate for calculating the absolute values of the yield stresses for fabricated polycrystalline bars.

Preferred orientation was observed to be important. Tensile samples of alloy 4 made from severely cold rolled and annealed stock with the tensile axis the same as the rolling direction had significantly lower yield stresses for the same heat treatment than the swaged and annealed bars. For example, rolled samples aged at 730°C and 625°C had yield stresses of 36,000 and 43,300 psi while the corresponding swaged bars had yields of 40,900 and 53,600 psi, respectively. Rolled stock of this material has been shown to have a [112] preferred orientation along the rolling direction[12,13] which is very near to the orientation

which gives a minimum value to $\bar{m}$, i.e., $\bar{m} \geq 2$. Samples of alloys 1-3 were fabricated by forging while alloy 4 samples were swaged. This difference in fabrication procedure could result in the slight difference in $\bar{m}$ observed in Tables II and III for the best data fit. Also, the elastic moduli of the structures which precipitate in alloys 1-3 are different from those of the structures which form in alloy 4 and it is extremely hard to account exactly for this difference without making experimental measurements on single crystals of these components. Because the slope of the yield stress versus the difference in the cubic lattice parameters plot is dependent on both $\bar{m}$ and the elastic constants, the use of an $\bar{m}$ to give the best data fit is intended to normalize the unknown differences in both texture and elastic moduli. The agreement without these corrections is good considering the uncertainty in estimating the elastic moduli for the precipitating structures. No attempt was made to correct for changes in moduli of structures which change composition at different aging temperatures.

The rolled samples discussed above were not quenched after aging while the swaged bars were, and therefore the 730°C rolled sample value of 36,000 psi is slightly larger than it would have been had the sample been quenched after aging. The effect of hardening during cooling from the aging temperature was markedly observed on samples aged at 800°C. Samples of alloy 4 aged and relatively slowly cooled had a maximum hardness of R_B82 while those quenched after the aging treatment had a maximum hardness of R_B69. Also, because the transformation is hard to control at high temperatures, it is probable that the peak of the yield versus aging time curve was not attained exactly for the 800°C sample of alloy 4 and this would explain why the 800°C yield stress appears to be low (cf. Fig. 6 and Table III).

Effect of Ordering

It was at first thought that long range ordering of the copper-poor structure (Ni_3Fe) was partially responsible for the increase in yield of alloys 1-3 after the 450°C treatments. Wakelin and Yates[14] have shown that Ni_3Fe with up to four atomic percent copper will order on slowly cooling from 510°C to 400°C. It is difficult to prove the presence of order in Ni_3Fe by x-ray or other techniques so it was not certain that the copper-poor structure did order at 450°C. However, the trend in the yield stress increase indicated by an order-strengthening theory[15] was not observed. That is, the increase in yield of the alloys aged at 450°C over those aged at 625°C did not show a large dependence on volume fraction of the ordered structure but instead exhibited a constant increase for all volume fractions (cf. Table II). This constant increase is consistent with the predictions of the present theory as is the calculated magnitude of the strength increase. To eliminate the complications of the ordering phenomena, alloy 4 was aged at four temperatures above the ordering temperature. The yield stress data for alloy 4 fit the theory nicely and therefore it is certain that the yield increase of alloys 1-3 aged at 450°C over those aged at 625°C is due to increased coherency strains and is not due to ordering. The strong possibility that ordering is occurring in the copper-poor structure at 450°C suggests that ordering of lamellar precipitates does not cause large strength increases. It is well-known that materials which will order do not show significant differences in yield stress between the unordered and the fully ordered state.

SUMMARY AND CONCLUSIONS

The yield stresses of polycrystalline Cu-Ni-Fe alloys were measured and compared with values calculated from the theory presented in Part I of this work.[1] Agreement between theory and experiment was found for the following points:

1. The yield stress is directly proportional to the difference in the cubic lattice parameters of the two structures forming the lamellar microstructure.

2. The yield stress is independent of the volume fractions of the structures present in the Cu-Ni-Fe alloys studied.

3. The yield stress is independent of the modulated structure wavelength present which means it is independent of interlamellar spacing.

In addition, calculations indicate that the demixing process of spinodal decomposition in Cu-Ni-Fe alloys is inhibited by the coherency strains created during decomposition. Finally, the possibility that ordering of the copper-poor structure was causing the observed strength increases was discounted.

ACKNOWLEDGEMENTS

The author wishes to thank Professor E. R. Parker for helpful discussions. This work is included in the author's Ph.D. thesis and was supported financially by the United States Atomic Energy Commission.

REFERENCES

1. Dahlgren, S. D., submitted to Acta Met.
2. Bradley, A. J., Proc. Phys. Soc., 52, 80 (1940).
3. Hargreaves, M. E., Acta Cryst., 4, 301 (1951).
4. Biedermann, E. and E. Kneller, Z. Metall., 47, 289 (1956).
5. Cottrell, A. H., Dislocations and Plastic Flow in Crystals, (Clarendon Press, Oxford, England, 1953) p. 116.
6. Köster, W., and W. Dannöhl, Z. Metall., 27, 220 (1935).
7. Daniel, V., Proc. Roy Soc., 192, 575 (1947).
8. Daniel, V. and H. Lipson, Proc. Roy. Soc, A181, 378 (1944).
9. Hillert, M., M. Cohen, and B. L. Averbach, Acta Met., 9, 536 (1961).
10. Bradley, A. J., W. F. Cox, and H. J. Goldschmidt, J. Inst. Metals, 67, 189 (1941).
11. Barrett, C. S., Structure of Metals, (McGraw-Hill Book Co., Inc., New York, 1952) p. 443.
12. Ibid., p. 499.
13. Ibid., p. 458.
14. Wakelin, R. J. and E. L. Yates, Proc. Phys. Soc., London B66, 221 (1953).
15. Williams, R. O., Acta Met., 5, 241 (1957).

FIGURE CAPTIONS

Fig. 1 Isothermal section for 600°C of the Cu-Ni-Fe phase diagram[6] showing the compositions of alloys 1-4 investigated in this study. Only the portion of interest away from the iron corner is included.

Fig. 2 Measured room temperature yield stress vs aging time at 625°C for alloy 2. Numbers in parentheses are approximate modulation wavelengths given in numbers of atomic planes.[9]

Fig. 3 Measured yield stresses for alloys 1-3 (circles) and alloy 4 (triangles) vs the difference in cubic lattice parameters of the precipitating structures. Squares represent values calculated for alloy 4 ($\bar{m} = 2.5$).

Fig. 4 Measured values of a_{10} (copper-poor structure) and a_{20} (copper-rich structure) are given as a function of the temperature and are designated by squares and solid lines. Values of a_{10} and a_{20} calculated from tetragonal lattice parameter data are given by circles and dashed lines.

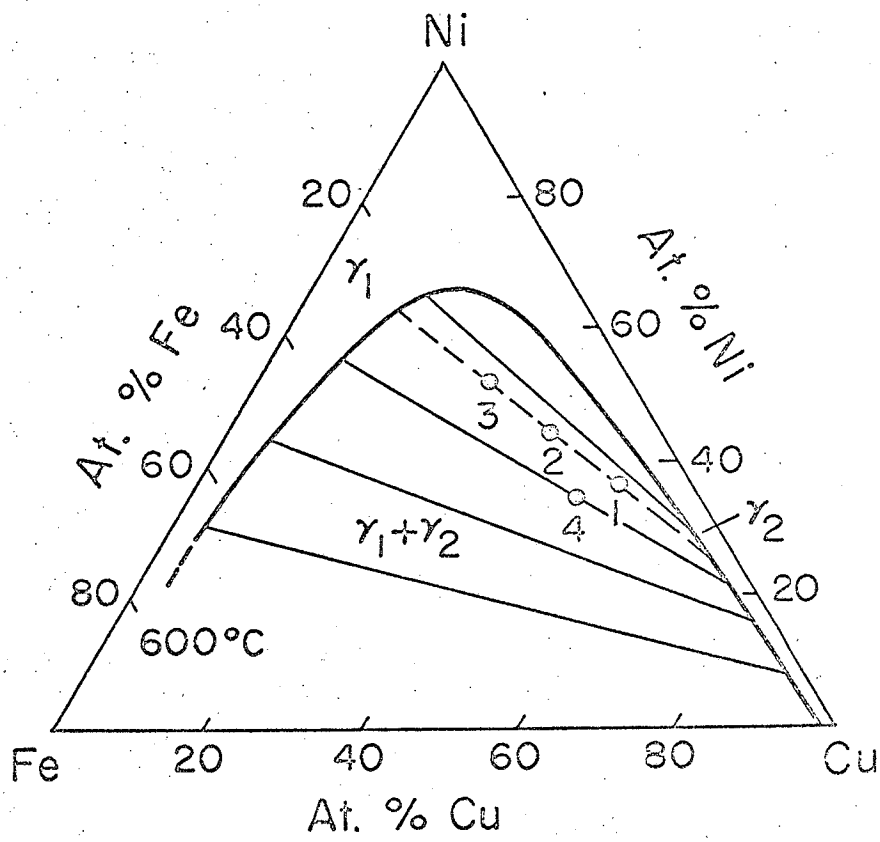

MUB-9676

Fig. 1

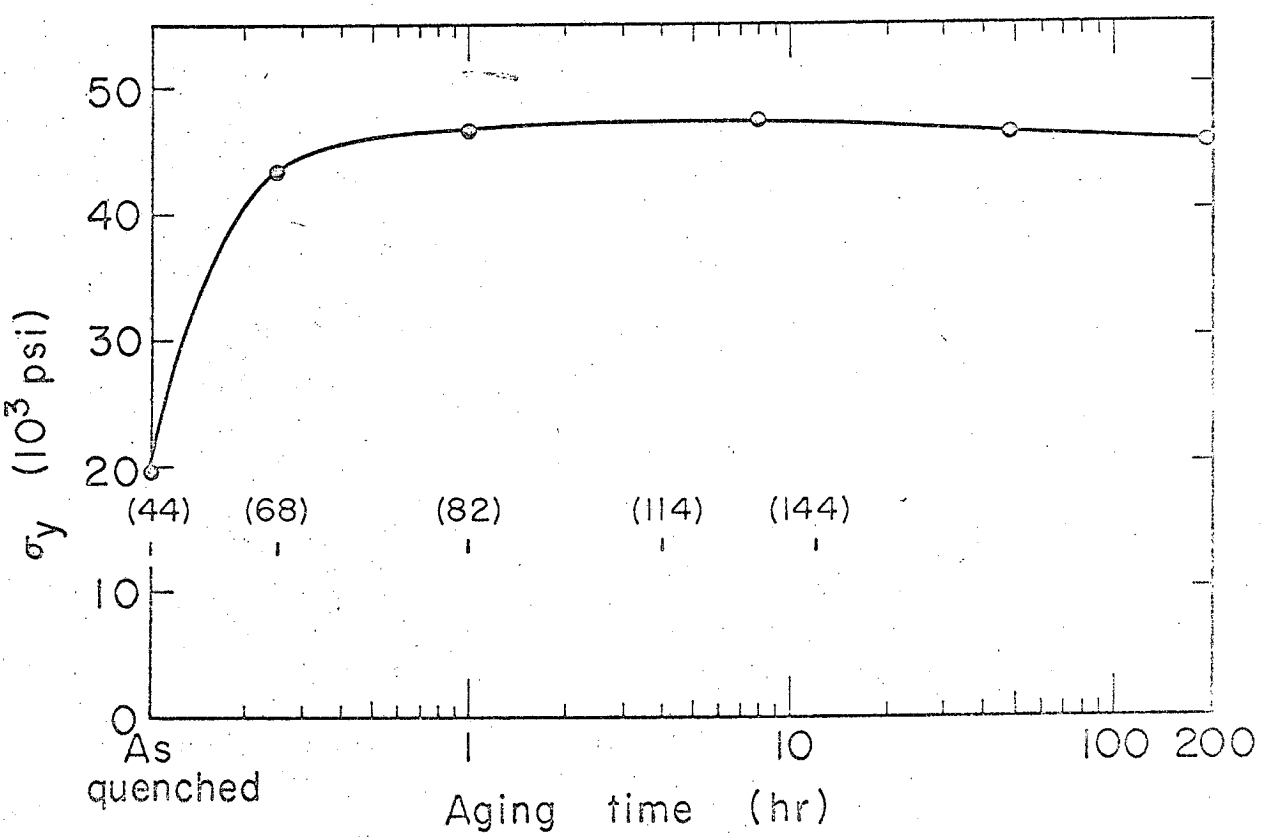

MUB-9675

Fig. 2

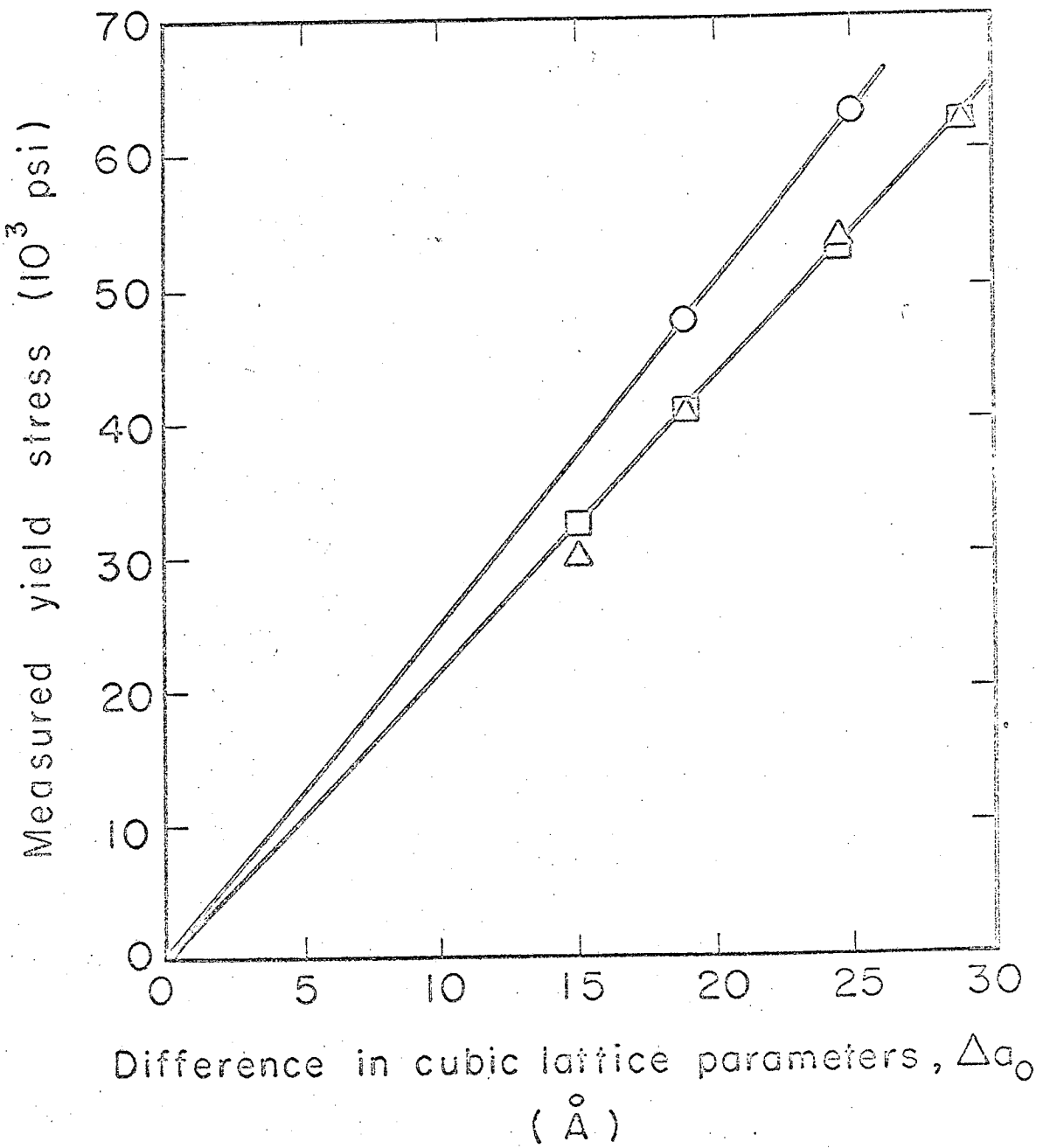

MUB-10538

Fig. 3

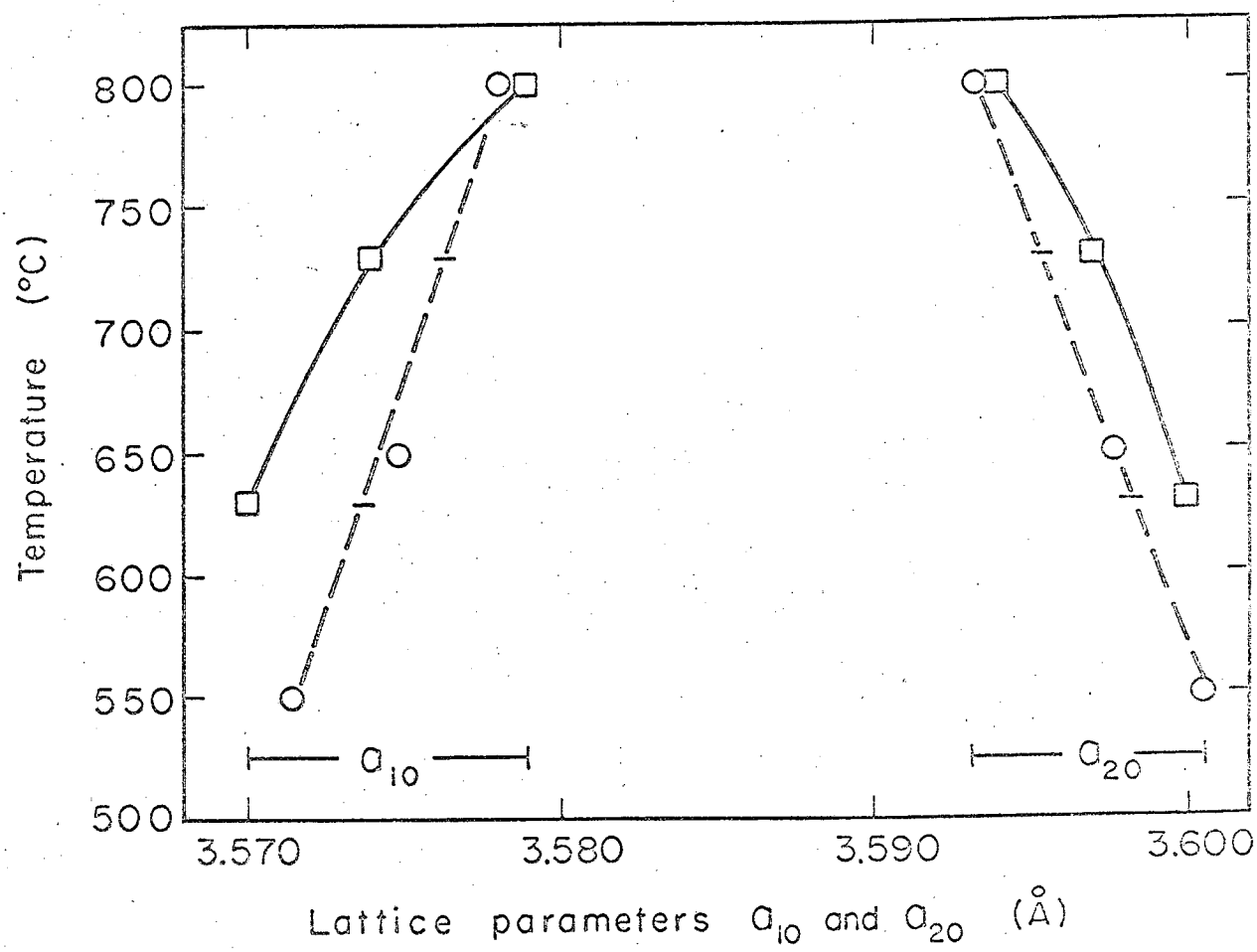

MUB-10537

Fig. 4

This report was prepared as an account of Government sponsored work. Neither the United States, nor the Commission, nor any person acting on behalf of the Commission:

A. Makes any warranty or representation, expressed or implied, with respect to the accuracy, completeness, or usefulness of the information contained in this report, or that the use of any information, apparatus, method, or process disclosed in this report may not infringe privately owned rights; or

B. Assumes any liabilities with respect to the use of, or for damages resulting from the use of any information, apparatus, method, or process disclosed in this report.

As used in the above, "person acting on behalf of the Commission" includes any employee or contractor of the Commission, or employee of such contractor, to the extent that such employee or contractor of the Commission, or employee of such contractor prepares, disseminates, or provides access to, any information pursuant to his employment or contract with the Commission, or his employment with such contractor.